Interaction of amyloid and tau on cortical microstructure in cognitively unimpaired adults

Nicholas M. Vogt[1], Jack V. F. Hunt[1], Nagesh Adluru[2], Yue Ma[1], Carol A. Van Hulle[1], Douglas C. Dean III[2,3,4], Nathaniel A. Chin[1], Cynthia M. Carlsson[1,5], Sanjay Asthana[1,5], Sterling C. Johnson[1,5], Henrik Zetterberg[6,7,8,9], Andrew L. Alexander[2,4], Kaj Blennow[6,7], Barbara B. Bendlin[1,*]

[1]Wisconsin Alzheimer's Disease Research Center, University of Wisconsin School of Medicine and Public Health, Madison, WI, USA

[2]Waisman Laboratory for Brain Imaging and Behavior, Waisman Center, University of Wisconsin-Madison, Madison, WI, USA

[3]Department of Pediatrics, University of Wisconsin School of Medicine and Public Health, Madison, WI, USA

[4]Department of Medical Physics, University of Wisconsin School of Medicine and Public Health, Madison, WI, USA

[5]Geriatric Research Education and Clinical Center, William S. Middleton Memorial Veterans Hospital, Madison, WI, USA

[6]Institute of Neuroscience and Physiology, Department of Psychiatry and Neurochemistry, The Sahlgrenska Academy at the University of Gothenburg, Mölndal, Sweden

[7]Clinical Neurochemistry Laboratory, Sahlgrenska University Hospital, Mölndal, Sweden

[8]Department of Neurodegenerative Disease, UCL Institute of Neurology, London, UK

[9]UK Dementia Research Institute at University College London, London, UK

***Corresponding author: Barbara Bendlin (bbb@medicine.wisc.edu)**

Abstract

Introduction: Neurite orientation dispersion and density imaging (NODDI), a multi-compartment diffusion-weighted imaging (DWI) model, may be useful for detecting early cortical microstructural alterations in Alzheimer's disease prior to cognitive impairment.

Methods: Using neuroimaging (NODDI and T1-weighted magnetic resonance imaging [MRI]) and cerebrospinal fluid (CSF) biomarker data (measured using Elecsys® CSF immunoassays) from 219 cognitively unimpaired participants, we tested the main and interactive effects of CSF amyloid beta (Aβ)42 /Aβ40 and phosphorylated tau (p-tau) on cortical NODDI metrics and cortical thickness, controlling for age, sex, and apolipoprotein E ε4.

Results: We observed a significant CSF Aβ42 /Aβ40 × p-tau interaction on cortical neurite density index (NDI), but not orientation dispersion index or cortical thickness. The directionality of these interactive effects indicated: (1) among individuals with lower CSF p-tau, greater amyloid burden was associated with higher cortical NDI; and (2) individuals with greater amyloid and p-tau burden had lower cortical NDI, consistent with cortical neurodegenerative changes.

Discussion: NDI is a particularly sensitive marker for early cortical changes that occur prior to gross atrophy or development of cognitive impairment.

Keywords: cerebrospinal fluid biomarkers; cortical microstructure; diffusion; magnetic resonance imaging; neurite orientation dispersion and density imaging; preclinical.

Introduction

In Alzheimer's disease, pathologic accumulation of amyloid-β (Aβ) and tau occurs for years prior to macroscopic neurodegenerative changes and subsequent cognitive impairment (Jack *et al.*, 2011, 2013; Buchhave *et al.*, 2012). Developing sensitive markers of neurodegeneration will be vital for improving understanding of the timing and progression of Alzheimer's disease, as well as identifying asymptomatic individuals at risk of developing cognitive decline, especially given that this prodromal period may be the most optimal time for therapeutic intervention (Mangialasche *et al.*, 2010; Gauthier *et al.*, 2015).

By measuring the diffusion of water molecules within tissues, diffusion-weighted imaging (DWI) provides the ability to assess neuronal microstructure *in vivo*, making it potentially more sensitive than conventional T1-weighted structural imaging for detecting early cortical changes associated with Alzheimer's disease pathology (Weston *et al.*, 2015). Recent advancements in multi-shell DWI acquisitions and multi-compartment modeling techniques have greatly improved the ability to study cortical microstructure (Assaf *et al.*, 2013; Fukutomi *et al.*, 2018). Neurite orientation dispersion and density imaging (NODDI) (Zhang *et al.*, 2012) is one such multi-compartment model in which the composite diffusion signal is subdivided into three microstructural compartments: isotropic diffusion (i.e. free water), intracellular diffusion (highly restricted diffusion in neurites), and extracellular diffusion (hindered diffusion outside neurites). These subcomponents are used to calculate two quantitative microstructural metrics: 1) neurite density index (NDI), or the volume fraction of intracellular (neurite) diffusion, and 2) orientation dispersion index (ODI), which reflects the degree of neurite coherence. An important aspect of NODDI is the modeling of free water (i.e. CSF), which helps account for partial volume effects and makes it particularly well-suited for investigating cortical microstructure, especially in neurodegenerative conditions.

Previous studies using the NODDI model to investigate cortical microstructural alterations in clinical Alzheimer's disease have demonstrated lower NDI and ODI across widespread cortical regions in both young onset and sporadic Alzheimer's disease participants (Parker *et al.*, 2018; Vogt *et al.*, 2020). Moreover, participants with mild cognitive impairment (MCI) had lower cortical NDI – but not cortical thickness – in several key regions affected early in Alzheimer's

disease, suggesting that NDI may be a sensitive marker of cortical microstructural alterations that occur prior to measurable cortical atrophy. However, whether cortical NODDI microstructure is associated with Alzheimer's disease pathology prior to development of cognitive impairment remains to be determined.

In this study, we tested the relationship between Alzheimer's disease pathology as indexed by cerebrospinal fluid (CSF) biomarkers and cortical NODDI microstructure in cognitively unimpaired late middle-aged adults. Specifically, we used whole-brain analyses to test the main and interactive effects of CSF Aβ and phosphorylated tau on both cortical NODDI metrics and cortical thickness, followed up with targeted region of interest (ROI) analyses in an Alzheimer's disease signature composite region to more directly compare the effects on cortical microstructure and cortical thickness.

Materials and Methods

Participants

We identified 219 cognitively unimpaired individuals from the Wisconsin Alzheimer's Disease Research Center (ADRC) clinical core (n = 131) and the Wisconsin Registry for Alzheimer's Prevention (WRAP) study (Johnson *et al.*, 2018) (n = 88) who had undergone both MRI acquisition (multi-shell DWI and T1-weighted) as well as lumbar puncture for CSF biomarker quantification. All participants underwent comprehensive neuropsychological testing to determine cognitive status. All ADRC participants are reviewed by a multidisciplinary consensus review committee consisting of physicians, neuropsychologists, and nurse practitioners. WRAP participants are selectively reviewed by the consensus review committee when cognitive abnormalities are detected by algorithm on neuropsychological tests (Johnson *et al.*, 2018). General exclusion criteria for the ADRC and WRAP studies include any significant neurologic disease (other than Alzheimer's disease dementia), history of alcohol/substance dependence, major psychiatric disorders (including untreated major depression), or other significant medical illness. The University of Wisconsin Health Sciences Institutional Review Board approved all study procedures and all participants provided written informed consent.

Lumbar Puncture and Cerebrospinal Fluid Analysis

CSF was collected via lumbar puncture in the morning after a minimum 4hr fast with a Sprotte 25- or 24-gauge spinal needle at the L3/4 or L4/5 interspace using gentle extraction into propylene syringes. CSF (~22 mL) was then combined, gently mixed and centrifuged at 2,000 x *g* for 10 minutes. Supernatants were frozen in 0.5 mL aliquots in polypropylene tubes and stored at −80 °C.

CSF $A\beta_{40}$, $A\beta_{42}$, and phosphorylated tau-181 (pTau) concentrations were measured on the Roche Elecsys® immunoassay platform (Bittner *et al.*, 2015; Lifke *et al.*, 2019). CSF amyloid burden was quantified by the $A\beta_{42}/A\beta_{40}$ ratio (lower CSF levels indicate greater amyloid burden), which shows better correspondence with brain amyloid deposition than CSF $A\beta_{42}$ alone (Lewczuk *et al.*, 2015). Cutoff values for CSF biomarkers were developed using receiver operating characteristic (ROC) curve analysis and Youden's J statistic as previously described (Clark *et al.*, 2018). The cutoff for CSF $A\beta_{42}/A\beta_{40}$ positivity was <0.044, and the cutoff for CSF pTau positivity was >24.04 pg/mL.

MRI Acquisition and Processing

MRI data were acquired using a General Electric 3T MR750 scanner with a 32-channel head coil. Diffusion-weighted images were acquired using a multi-shell spin-echo echo-planar imaging pulse sequence (6 x b = 0 s/mm^2, 9 x b = 500 s/mm^2, 18 x b = 800 s/mm^2, and 36 x b = 2000 s/mm^2; TR/TE = 8575/76.8 ms; 2x2x2 mm^3 isotropic voxel resolution; 128 x 128 acquisition matrix). T1-weighted structural images were acquired using a 3D inversion recovery prepared fast spoiled gradient-echo FSPGR-BRAVO sequence (TI = 450 ms; TR/TE = 8.1/3.2 ms; flip angle = 12°; 1x1x1 mm^3 isotropic voxel resolution; 256 x 256 acquisition matrix).

Diffusion-weighted images underwent denoising (Veraart *et al.*, 2016), Gibbs ringing correction (Kellner *et al.*, 2016), and motion and eddy current correction (Andersson and Sotiropoulos, 2016). Fractional anisotropy (FA) maps were fit using Diffusion Imaging in Python (DIPY) (Garyfallidis *et al.*, 2014), and subsequently segmented into white matter (WM) fraction maps using *Atropos* (Avants *et al.*, 2011b) in ANTs (Avants *et al.*, 2011a). NODDI parameter maps (neurite density index [NDI], orientation dispersion index [ODI], and isotropic volume fraction [V_{ISO}]) were fit using Accelerated Microstructure Imaging via Convex Optimization (AMICO) (Daducci *et al.*,

2015) with an optimized intracellular intrinsic parallel diffusivity parameter ($d_{\parallel}$) of 1.1 μm^2/ms to improve fit in gray matter (Fukutomi *et al.*, 2018; Guerrero *et al.*, 2019). All diffusion images were visually inspected prior to further analyses.

T1-weighted structural images were processed using the Computational Anatomy Toolbox (CAT12, http://www.neuro.uni-jena.de/cat/) in SPM12 (https://www.fil.ion.ucl.ac.uk/spm/). Cortical thickness was estimated using the projection-based thickness (PBT) method (Dahnke *et al.*, 2013), followed by topological correction (Yotter *et al.*, 2011a) and spherical mapping and registration (Yotter *et al.*, 2011b). Prior to vertex-wise analyses, surface data were resampled into template space (32k mesh resolution; ~2 mm average vertex spacing) (Glasser *et al.*, 2013) and smoothed using the default 15 mm FWHM filter size. All CAT12 segmentations and cortical surface meshes were visually inspected prior to further analyses.

Gray Matter-Based Spatial Statistics (GBSS) Processing

GBSS uses the tract-based spatial statistics (TBSS) framework (Smith *et al.*, 2006) to allow for unbiased gray matter-specific voxel-wise statistical analysis of cortical microstructure (Nazeri *et al.*, 2015). Processing steps for GBSS have been previously described (Nazeri *et al.*, 2015, 2017; Vogt *et al.*, 2020). Briefly, for each participant, a gray matter (GM) fraction map was generated by subtracting the WM fraction map (estimated from the participant's FA map using 2 tissue segmentation in *Atropos*) and the CSF fraction map (estimated from the participant's NODDI V_{ISO} parameter map) from 1. The GM, WM, and CSF fraction maps were then combined to generate a "pseudo T1-weighted" image. Pseudo T1-weighted images from all participants were then used to create a common voxel space population template via iterative nonlinear registration in ANTs. The warp fields generated from this step were then used to nonlinearly warp NDI, ODI, and GM fraction images for each participant into the population template space. GM fraction images in population template space were averaged to generate a mean GM image, which was then skeletonized using FSL's *tbss_skeleton* tool. Finally, NDI and ODI were projected onto the GM skeleton from the local GM fraction maxima, and the GM skeleton was thresholded to only include voxels with GM fraction > 0.65 in > 70% of participants.

Alzheimer's Disease Signature Composite Region Processing

In order to compare effects for both cortical microstructure and cortical thickness within the same brain regions, an Alzheimer's disease signature composite ROI was constructed using the Desikan atlas (Desikan *et al.*, 2006; Klein and Tourville, 2012) and included bilateral inferior parietal, middle temporal, inferior temporal, precuneus, fusiform, and entorhinal subregions (Schwarz *et al.*, 2016). For cortical microstructure, a T1-weighted atlas-space image was nonlinearly registered to each participant's pseudo T1 image, and the resulting warp fields were used to transform binarized subregion ROIs into native diffusion space. Subregion ROIs were masked by the participant's GM fraction map (thresholded at 0.7 and binarized) to ensure ROIs only included GM voxels. Volume (estimated by number of voxels) and microstructural metrics were extracted within each GM-masked subregion and used to calculate a weighted averaged for the Alzheimer's signature composite region (weighted by relative subregion volume to account for differences in ROI subregion size). For cortical thickness, mean cortical thickness within each subregion was extracted using ROI tools in CAT12 and averaged to calculate mean cortical thickness within the overall Alzheimer's composite region.

Statistical Analysis

We first performed whole-brain analyses to determine the main and interactive effects of CSF $A\beta_{42}/A\beta_{40}$ and pTau on cortical NODDI metrics and cortical thickness. Voxel-wise GBSS analyses were performed on the final skeletonized population-space NDI and ODI images using nonparametric permutation inference (n = 10,000 permutations) with threshold-free cluster enhancement (TFCE) (Smith and Nichols, 2009) in FSL's *randomise* (Winkler *et al.*, 2014). Vertex-wise cortical thickness analyses were performed using the resampled and smoothed surface data and FSL's *Permutation Analysis of Linear Models (PALM)* tool (n = 10,000 permutations) with TFCE. Resulting statistical maps were family-wise error (FWE)-corrected at $P_{FWE} < 0.05$ and displayed as surfaces using *Surf Ice* (https://www.nitrc.org/projects/surfice/). CSF $A\beta_{42}/A\beta_{40}$ and pTau values were treated as continuous variables (pTau was $\log_{10}$-transformed due to non-normality), and all statistical models included age and sex as covariates using the following formula:

$$\text{NODDI microstructure OR cortical thickness} = \beta_0 + \beta_1*\text{Age} + \beta_2*\text{Sex} + \beta_3*A\beta_{42}/A\beta_{40} + \beta_4*\text{pTau} + \beta_5*(A\beta_{42}/A\beta_{40} \times \text{pTau}) + \varepsilon$$

In order to determine the directionality of $A\beta_{42}/A\beta_{40}$ × pTau interaction effects, significant voxels from GBSS statistical maps were deprojected and warped back into each participant's native diffusion space, and mean values across all significant voxels were extracted from native space NODDI parameter maps for each participant. These values were then used for scatterplots and simple slopes analyses using the *interactions* package (version 1.1.1) in R to examine continuous by continuous interactions. In simple slopes analyses, conditional slopes are estimated to test whether the relationship between predictor and outcome variables is significant at a given level of the moderator variable. Separate tests evaluated both $A\beta_{42}/A\beta_{40}$ and pTau as moderators, and in order to facilitate interpretation of simple slope results, two moderator levels were chosen based on CSF biomarker cutoff groupings (e.g. Aβ- and Aβ+; pTau- and pTau+). Specifically, simple slopes analyses tested: 1) the relationship between $A\beta_{42}/A\beta_{40}$ and NODDI metrics at mean pTau levels of both the pTau- and pTau+ groups; and 2) the relationship between pTau and NODDI metrics at mean $A\beta_{42}/A\beta_{40}$ levels of both the Aβ+ and Aβ- groups. Finally, participants were classified into four biomarker groups (A-/T-, A-/T+, A+/T-, A+/T+) based on dichotomous CSF $A\beta_{42}/A\beta_{40}$ and pTau cutoffs, and differences in NODDI metrics between groups were tested using ANCOVA models (age and sex included as covariates).

To more directly compare microstructure and cortical thickness, we tested the main and interactive effects of $A\beta_{42}/A\beta_{40}$ and pTau on NODDI metrics or cortical thickness within the Alzheimer's signature composite region (Schwarz *et al.*, 2016). Linear regression models were identical to those used in whole-brain analyses, and once again, scatter plots and simple slopes analyses were used to determine the directionality of the continuous by continuous $A\beta_{42}/A\beta_{40}$ × pTau interaction effects. Finally, we examined the regional patterns of $A\beta_{42}/A\beta_{40}$ × pTau interaction effects on NODDI microstructure by performing simple slopes analyses on each Alzheimer's composite subregion separately.

Data availability

The datasets used for the current study are available from the corresponding author on reasonable request.

Results

Participant Characteristics

Participant characteristics are presented in Table 1.

Table 1. Participant characteristics

Characteristic	Value
N	219
Age at MRI, years (mean ± SD)	66.8 ± 7.5
Age at LP, years (mean ± SD)	64.9 ± 7.5
Age difference between MRI and LP, years (median [IQR])	1.21 [0-4.03]
Sex, % female (*n*)	58.9% (129/219)
APOE ε4 genotype, % positive (*n*)	34.9% (76/219)
Primary race/ethnicity, *n* (Caucasian/African American/Asian/Native American/Other)	213 / 3 / 1 / 1 / 1
Education, years (mean ± SD)	16.6 ± 2.3
CSF values	
$A\beta_{40}$, ng/mL (mean ± SD)	14.8 ± 4.6
$A\beta_{42}$, pg/mL (mean ± SD)	908 ± 389
$A\beta_{42}/A\beta_{40}$ (mean ± SD)	0.06 ± 0.02
pTau, pg/mL (median [IQR])	16.9 [13.3-22.1]
CSF biomarker cutoff groups, *n* (% of sample)	
A-/T-	166 (75.8%)
A-/T+	13 (5.9%)
A+/T-	18 (8.2%)
A+/T+	22 (10.0%)

Whole-Brain Voxel- and Vertex-Wise Analyses

Whole-brain analyses demonstrated a significant $A\beta_{42}/A\beta_{40}$ × pTau interaction on NDI that was distributed predominantly throughout temporal, parietal, and medial frontal cortical regions (Fig. 1A; Supplementary Fig. 1). This finding was most prominent in the right inferior parietal region (including angular and supramarginal gyrus), bilateral posterior middle temporal region, temporal

pole, entorhinal region, and posterior cingulate. There were no subcortical gray matter regions with significant $A\beta_{42}/A\beta_{40}$ × pTau interaction on NDI. There was no significant $A\beta_{42}/A\beta_{40}$ × pTau interaction on ODI or cortical thickness, and there were no significant main effects of $A\beta_{42}/A\beta_{40}$ or pTau on NDI, ODI, or cortical thickness.

NDI values were extracted from significant GBSS voxels in native diffusion space and used in linear regression models followed by simple slopes analysis in order to investigate the directionality of the continuous by continuous interaction effect of $A\beta_{42}/A\beta_{40}$ × pTau. As expected, there was a significant $A\beta_{42}/A\beta_{40}$ × pTau interaction on NDI values from significant GBSS voxels (β = 1.46, 95% CI 0.98 to 1.94, $P < 0.0001$). Using the mean values of pTau in the pTau- group (15.9 pg/mL) and pTau+ group (31.2 pg/mL), there was a significant negative conditional slope of $A\beta_{42}/A\beta_{40}$ on NDI at the pTau- group mean (β = -0.22, 95% CI -0.33 to -0.12, $P < 0.0001$; Fig. 1B) and a significant positive conditional slope at the pTau+ group mean (β = 0.22, 95% CI 0.11 to 0.33, $P < 0.0001$; Fig. 1B). Similarly, using the mean values of $A\beta_{42}/A\beta_{40}$ in the Aβ- group (0.068) and Aβ+ group (0.033), there was a significant positive conditional slope of pTau on NDI at the Aβ- group mean (β = 0.011, 95% CI 0.001 to 0.020, $P = 0.0298$; Fig. 2C) and a significant negative conditional slope at the Aβ+ group mean (β = -0.040, 95% CI -0.055 to -0.026, $P < 0.0001$; Fig. 1C).

Finally, after collapsing participants into four biomarker groups based on dichotomous $A\beta_{42}/A\beta_{40}$ and pTau cutoffs, ANCOVA models using NDI values from significant GBSS voxels demonstrated significant differences in cortical NDI between biomarker groups ($F_{213} = 3.66$, $P = 0.0034$; Fig. 1D). Specifically, *post hoc* comparisons indicated that while A-/T- and A-/T+ groups did not differ, the A+/T- group had higher NDI than the A-/T- group, and the A+/T+ group had lower NDI than all other groups.

Alzheimer's Disease Composite Region Analyses

Within the Alzheimer's disease composite region, there was a significant $A\beta_{42}/A\beta_{40}$ × pTau interaction on NDI (β = 0.83, 95% CI 0.35 to 1.31, $P = 0.00069$; Fig. 2A&B), but not cortical thickness (β = 2.32, 95% CI -5.4 to 10.1, $P = 0.56$; Fig. 2C&D). Specifically, examining Aβ × pTau status using simple slopes analysis indicated that there was a significant negative conditional

slope of $A\beta_{42}/A\beta_{40}$ on NDI at the pTau- group mean (β = -0.14, 95% CI -0.24 to -0.03, *P* = 0.012; Fig. 2A) and a significant positive conditional slope at the pTau+ group mean (β = 0.12, 95% CI 0.01 to 0.23, *P* = 0.031; Fig. 2A). Examining pTau × Aβ status using simple slopes analysis indicated that while the conditional slope of pTau on NDI at the Aβ- group mean was not significant (β = 0.005, 95% CI -0.004 to 0.015, *P* = 0.29; Fig. 2B), there was a significant negative conditional slope of pTau on NDI at the Aβ+ group mean (β = -0.024, 95% CI -0.039 to -0.009, *P* = 0.0017; Fig. 2B). Similar results were observed in simpler interaction models where $A\beta_{42}/A\beta_{40}$ was kept continuous and pTau was dichotomized, and where pTau was kept continuous and $A\beta_{42}/A\beta_{40}$ was dichotomized (see Supplementary material). There were no main effects of $A\beta_{42}/A\beta_{40}$ or pTau on NDI or cortical thickness within the Alzheimer's disease composite region.

Overall, the GBSS and Alzheimer's composite region results indicate an $A\beta_{42}/A\beta_{40}$ × pTau interaction effect on cortical microstructure in which lower levels of CSF $A\beta_{42}/A\beta_{40}$ (i.e. greater amyloid burden) in pTau- individuals were associated with higher cortical NDI. Additionally, lower levels of CSF $A\beta_{42}/A\beta_{40}$ in pTau+ individuals, as well as higher levels of CSF pTau in Aβ+ individuals, were both associated with lower cortical NDI.

Alzheimer's Disease Composite Subregion Analyses

We performed simple slopes analyses on the Alzheimer's composite subregions in order to investigate the regional patterns of $A\beta_{42}/A\beta_{40}$ × pTau interaction effects on NDI. For Aβ × pTau status, all subregions had negative conditional slopes of $A\beta_{42}/A\beta_{40}$ on NDI at the pTau- group mean and positive conditional slopes of $A\beta_{42}/A\beta_{40}$ on NDI at the pTau+ group mean (Fig. 3A). At the pTau- group mean, conditional slopes were significant ($P < 0.05$, uncorrected) in right inferior parietal, right middle temporal, bilateral inferior temporal, bilateral fusiform, and bilateral entorhinal subregions, indicating that greater amyloid burden was associated with higher NDI in these subregions for individuals who were pTau-. At the pTau+ group mean, conditional slopes were significant in right inferior parietal, right middle temporal, bilateral inferior temporal, and left precuneus subregions, indicating that greater amyloid burden was associated with lower NDI in these subregions for individuals who were pTau+.

For pTau × Aβ status, conditional slopes of pTau on NDI at the Aβ- group mean were close to zero for all subregions, with the exception of the left inferior temporal subregion, which had a significant positive conditional slope (Fig. 3B). However, at the Aβ+ group mean, nearly all subregions had significant negative conditional slopes of pTau on NDI (with the exception of the entorhinal subregion), indicating that higher levels of CSF pTau were associated with lower NDI in nearly every Alzheimer's composite subregion for Aβ+ individuals.

Discussion

Hypothetical models describing the temporal ordering of biomarker abnormalities along the continuum of Alzheimer's disease propose sequential detectable changes in amyloid, tau, and then neurodegeneration (Jack *et al.*, 2013). While conventional T1-weighted MRI-derived macrostructural measures (e.g. cortical thickness or gray matter volume) are often used as markers of neurodegenerative changes, recent work has proposed that microstructural features of neurodegeneration should also be considered on this continuum and may be detectable prior to macrostructural changes (Weston *et al.*, 2015). Here, we examined the extent to which Alzheimer's associated neurodegeneration is detectable in the preclinical asymptomatic phase of the disease using multi-shell DWI, and found that indeed, microstructural alterations, especially altered neurite density, were present among cognitively unimpaired individuals with amyloid and tau pathology. Moreover, there were no changes observed when using the T1-weighted derived measure of cortical thickness, suggesting that DWI microstructural metrics are more sensitive than macrostructural features for detecting early cortical neurodegenerative changes in preclinical Alzheimer's disease.

Previous studies have reported alterations in cortical NODDI microstructure for individuals with both clinical Alzheimer's disease dementia and mild cognitive impairment (Parker *et al.*, 2018; Vogt *et al.*, 2020). Here, we find that altered cortical neurite density is also present in the preclinical, asymptomatic phase of the disease. Specifically, we observed that greater amyloid burden (indexed by lower CSF $A\beta_{42}/A\beta_{40}$ levels) was associated with higher cortical NDI, but only when CSF pTau was low, suggesting an earlier disease stage. Secondly, we observed that greater amyloid burden accompanied by higher tau pathology was associated with lower NDI, suggesting loss of cortical neurites with worsening Alzheimer's disease pathology. These findings were

observed in both whole-brain voxel-wise GBSS analyses and in follow-up targeted analyses using NDI values extracted in native diffusion space from Alzheimer's disease-specific cortical regions. Together, these findings suggest a non-monotonic relationship between cortical NDI and progression of Alzheimer's disease pathology, where early amyloid deposition is associated with restricted intracellular diffusion, and subsequent accumulation of pathology is associated with less restricted intracellular diffusion, suggestive of neurite loss.

Several studies indicate that amyloid alone is often insufficient to induce clinical manifestation of Alzheimer's disease (Sperling *et al.*, 2011; Chételat *et al.*, 2013), and recent studies have demonstrated that both amyloid and tau are necessary for longitudinal cognitive decline in cognitively unimpaired individuals (Aschenbrenner *et al.*, 2018; Sperling *et al.*, 2018; Betthauser *et al.*, 2019; Jack *et al.*, 2019). Investigating the extent to which amyloid and tau pathology interact to impact alterations in brain structure in asymptomatic individuals is critical to improving the timing of clinical interventions, as well as improving the understanding of preclinical Alzheimer's progression. Due to its sensitivity to disruption in tissue barriers, DWI has been proposed as a more sensitive marker of cortical changes in Alzheimer's disease than conventional T1-weighted imaging (Weston *et al.*, 2015). The most commonly used DWI technique is diffusion tensor imaging (DTI), which models the diffusion signal as a simple ellipsoid tensor (Alger, 2012). A limited number of previous studies have used DTI (and specifically the metric of mean diffusivity [MD]) to investigate cortical microstructure in preclinical familial (Fortea *et al.*, 2010) and preclinical sporadic Alzheimer's disease (Montal *et al.*, 2018). These studies were instrumental in demonstrating a biphasic trajectory of cortical microstructure in asymptomatic individuals in which cortical MD was lower in A+/T- individuals and higher in A+/T+ individuals relative to A-/T- individuals. In the current study, we used the multi-compartment NODDI model and observed consistent results, whereby intracellular diffusion was highly restricted in the presence of amyloid, followed by less restricted intracellular diffusion among individuals with greater disease severity.

A major advantage of NODDI is the more complex and biologically relevant multi-compartment modeling of the diffusion signal. NODDI metrics may capture microstructural properties and quantify neuronal cytoarchitecture better than DTI metrics, which fail to capture several aspects of complex tissue microstructure (Pierpaoli *et al.*, 1996; Fukutomi *et al.*, 2018). Furthermore, by

directly modeling isotropic diffusion (i.e. free water), NODDI helps account for partial volume effects, which are of particular concern in neurodegenerative diseases where cortical atrophy can cause contamination of the diffusion signal from adjacent CSF and result in overestimation of MD changes (Weston *et al.*, 2015; Henf *et al.*, 2018). Previous studies have shown that cortical thickness and MD are highly correlated across almost the entire cerebral cortex (Jacobs *et al.*, 2013; Montal *et al.*, 2018). In the current study, there was no significant association between cortical thickness and NDI in the Alzheimer's disease composite region (Pearson's $r = 0.10$, 95% CI -0.03 to 0.23, $P = 0.13$), which suggests that cortical NDI quantifies meaningful microstructural changes associated with Alzheimer's disease pathology that are independent of alterations in cortical thickness and less influenced by partial voluming.

Microstructural alterations underlying higher or lower NDI may reflect multiple pathological processes occurring in Alzheimer's disease. Previous studies in animal models of Alzheimer's disease indicate that both Aβ deposition and neuroinflammation are associated with higher NDI (Colon-Perez *et al.*, 2019) and other multi-shell DWI markers of highly restricted diffusion (Vanhoutte *et al.*, 2013; Praet *et al.*, 2018). Additionally, higher NDI may reflect neuronal hypertrophy in response to amyloid deposition (Riudavets *et al.*, 2007; Iacono *et al.*, 2008, 2009). On the other end of the spectrum, lower NDI likely reflects loss of cellular barriers, reduction in myelinated axon density (Jespersen *et al.*, 2010; Grussu *et al.*, 2017; Fukutomi *et al.*, 2018), and loss of synapses and dendrites (Baloyannis *et al.*, 2011; Scheff *et al.*, 2011), all of which occur with accumulation of Alzheimer's disease pathology. Thus, in context of our current findings, changes in NDI likely reflect different stages of pathological processes that occur during the asymptomatic, preclinical phase of the disease. Subregion analyses demonstrated that differential changes in NDI were most pronounced in bilateral fusiform and inferior temporal subregions, which suggests that microstructural alterations in these regions may be more sensitive to accumulation of pathology. Histopathological correlation is required to further characterize these associations.

In the current study, while Alzheimer's disease pathology was associated with altered cortical NDI, we did not observe significant main or interactive effects of CSF $A\beta_{42}/A\beta_{40}$ and pTau on cortical thickness or ODI. While the question of whether amyloid alone has an impact on brain structure

has been controversial (Chételat *et al.*, 2013), several previous studies have shown a synergistic effect of amyloid and tau on decreased cortical thickness in preclinical Alzheimer's disease (Desikan *et al.*, 2011; Fortea *et al.*, 2014; Pegueroles *et al.*, 2016; Mak *et al.*, 2018; Montal *et al.*, 2018). It is worth noting that the individuals included in our current study were largely younger (66.8±7.5 years at DWI) compared to other preclinical Alzheimer's disease cohort studies (typically early to mid 70s), which may explain the lack of observed effects on cortical thickness. Therefore, detecting alterations in NDI but not cortical thickness in our younger cohort highlights the utility of NODDI metrics as sensitive markers of early cortical changes associated with Alzheimer's disease pathology. Additionally, previous studies have reported lower cortical ODI in individuals with clinical Alzheimer's disease dementia, but not individuals with MCI (Parker *et al.*, 2018; Vogt *et al.*, 2020). The current study provides further evidence that reductions in cortical ODI, which may reflect complexity of dendritic arborization (Grussu *et al.*, 2017; Fukutomi *et al.*, 2018), are observed in the later stages of disease severity when overt clinical dementia is present.

Several limitations of the current study should be noted. First, while the study included a large sample of well-characterized cognitively unimpaired participants, the analyses were cross-sectional. Longitudinal studies are needed to determine how Alzheimer's disease pathology impacts changes in cortical NODDI microstructure over time, both in preclinical and clinical populations. Second, while CSF $A\beta_{42}/A\beta_{40}$ and pTau provide good sensitivity and dynamic range, especially in asymptomatic individuals, they inherently do not provide regional information regarding accumulation of pathology. In particular, CSF pTau likely does not reflect accumulation of tangle pathology in our preclinical population, and more likely reflects increased tau phosphorylation and secretion as a neuronal response to amyloid accumulation (Joie *et al.*, 2017; Mattsson *et al.*, 2017; Barthélemy *et al.*, 2020). Future studies combining PET imaging biomarkers of amyloid and tau with NODDI are needed to better characterize the regional relationships between amyloid deposition, tau accumulation, and cortical NODDI microstructure.

Conclusion

In combination with previous studies of NODDI-derived measures of microstructure in symptomatic Alzheimer's disease, the current results demonstrate that NODDI is a powerful tool for characterizing cortical microstructural alterations along the continuum of Alzheimer's disease.

Specifically, in preclinical Alzheimer's disease, initial amyloid accumulation is associated with higher NDI, while subsequent further accumulation of amyloid and tau pathology is associated with lower NDI. In the symptomatic phase of the disease, several key early Alzheimer's disease cortical regions show lower NDI in individuals with MCI, while both NDI and ODI are lower across widespread cortical areas in individuals with clinical Alzheimer's disease dementia (Parker *et al.*, 2018; Vogt *et al.*, 2020). Notably, changes in NDI seem to occur prior to reliably detectable changes in cortical thickness. In the context of the recently proposed AT(N) Alzheimer's research framework (Jack *et al.*, 2018), these findings suggest that cortical NODDI metrics provide unique insights into the underlying cytoarchitectural changes occurring throughout disease progression, and may be particularly informative biomarkers of neurodegenerative changes (or "N"). Future work investigating how NODDI metrics are related to cognitive decline or predict conversion to MCI or clinical dementia will be vital for further characterizing cortical microstructural alterations in Alzheimer's disease.

Acknowledgements

We would like to extend our thanks to the committed research participants at the UW ADRC who make this work possible, as well as the staff and researchers at the University of Wisconsin ADRC for their assistance in study organization, participant recruitment, and facilitating data availability.

Funding

This research was supported by NIH grants F30AG059346 (to NMV), R01AG037639 (to BBB), R01AG027161 (to SCJ), P30 AG033514 (to SA), and the Geriatric Research, Education, and Clinical Center of the William S. Middleton Memorial Veterans Hospital. Additional support is provided by a core grant to the Waisman Center from the National Institute of Child Health and Human Development U54 HD090256 (to NA), the BRAIN Initiative R01EB022883 (to NA), and University of Wisconsin Center for Predictive Computational Phenotyping AI117924 (to NA). HZ is a Wallenberg Scholar supported by grants from the Swedish Research Council (#2018-02532), the European Research Council (#681712), the Swedish state under the agreement between the Swedish government and the County Councils, the ALF-agreement (#ALFGBG-720931), the Alzheimer Drug Discovery Foundation (ADDF), USA (#201809-2016862), and the UK Dementia Research Institute at UCL.

Competing Interests

HZ has served at scientific advisory boards for Denali, Roche Diagnostics, Wave, Samumed and CogRx, has given lectures in symposia sponsored by Fujirebio, Alzecure and Biogen, and is a co-founder of Brain Biomarker Solutions in Gothenburg AB (BBS), which is a part of the GU Ventures Incubator Program (all outside submitted work). The other authors report no competing interests.

Supplementary Material

Supplementary Figure 1. Axial slices of gray matter-based spatial statistics (GBSS) results for NDI.

Supplementary Table 1. Summary of interaction models for Alzheimer's disease composite region using dichotomous pTau and continuous $A\beta_{42}/A\beta_{40}$, as well as dichotomous $A\beta_{42}/A\beta_{40}$ and continuous pTau.

References

Alger JR. The diffusion tensor imaging toolbox. J Neurosci 2012; 32: 7418–7428.

Andersson JLR, Sotiropoulos SN. An integrated approach to correction for off-resonance effects and subject movement in diffusion MR imaging. Neuroimage 2016; 125: 1063–1078.

Aschenbrenner AJ, Gordon BA, Benzinger TLS, Morris JC, Hassenstab JJ. Influence of tau PET, amyloid PET, and hippocampal volume on cognition in Alzheimer disease. Neurology 2018; 91: e859–e866.

Assaf Y, Alexander DC, Jones DK, Bizzi A, Behrens TEJ, Clark CA, et al. The CONNECT project: Combining macro- and micro-structure. Neuroimage 2013; 80: 273–282.

Avants BB, Tustison NJ, Song G, Cook PA, Klein A, Gee JC. A reproducible evaluation of ANTs similarity metric performance in brain image registration. Neuroimage 2011a; 54: 2033–2044.

Avants BB, Tustison NJ, Wu J, Cook PA, Gee JC. An Open Source Multivariate Framework for n-Tissue Segmentation with Evaluation on Public Data. Neuroinformatics 2011b; 9: 381–400.

Baloyannis SJ, Manolides SL, Manolides LS. Dendritic and spinal pathology in the acoustic cortex in Alzheimer's disease: Morphological estimation in Golgi technique and electron microscopy. Acta Oto-laryngol 2011; 131: 610–612.

Barthélemy NR, Li Y, Joseph-Mathurin N, Gordon BA, Hassenstab J, Benzinger TammieLS, et al. A soluble phosphorylated tau signature links tau, amyloid and the evolution of stages of dominantly inherited Alzheimer's disease. Nat Med 2020; 26: 398–407.

Betthauser TJ, Koscik RL, Jonaitis EM, Allison SL, Cody KA, Erickson CM, et al. Amyloid and tau imaging biomarkers explain cognitive decline from late middle-age. Brain 2019; 143: 320–335.

Bittner T, Zetterberg H, Teunissen CE, Ostlund RE, Militello M, Andreasson U, et al. Technical performance of a novel, fully automated electrochemiluminescence immunoassay for the quantitation of β-amyloid (1-42) in human cerebrospinal fluid. Alzheimer's Dementia 2015; 12: 517–526.

Buchhave P, Minthon L, Zetterberg H, Wallin AK, Blennow K, Hansson O. Cerebrospinal fluid levels of β-amyloid 1-42, but not of tau, are fully changed already 5 to 10 years before the onset of Alzheimer dementia. Arch Gen Psychiat 2012; 69: 98–106.

Chételat G, Joie RL, Villain N, Perrotin A, Sayette V de L, Eustache F, et al. Amyloid imaging in cognitively normal individuals, at-risk populations and preclinical Alzheimer's disease. Neuroimage Clin 2013; 2: 356 365.

Clark LR, Berman SE, Norton D, Koscik RL, Jonaitis E, Blennow K, et al. Age-accelerated cognitive decline in asymptomatic adults with CSF β-amyloid. Neurology 2018; 90: e1306–e1315.

Colon-Perez LM, Ibanez KR, Suarez M, Torroella K, Acuna K, Ofori E, et al. Neurite orientation dispersion and density imaging reveals white matter and hippocampal microstructure changes produced by Interleukin-6 in the TgCRND8 mouse model of amyloidosis. Neuroimage 2019; 202: 116138.

Daducci A, Canales-Rodríguez EJ, Zhang H, Dyrby TB, Alexander DC, Thiran J-P. Accelerated Microstructure Imaging via Convex Optimization (AMICO) from diffusion MRI data. Neuroimage 2015; 105: 32–44.

Dahnke R, Yotter RA, Gaser C. Cortical thickness and central surface estimation. Neuroimage 2013; 65: 336–348.

Desikan RS, McEvoy LK, Thompson WK, Holland D, Roddey JC, Blennow K, et al. Amyloid-β associated volume loss occurs only in the presence of phospho-tau. Ann Neurol 2011; 70: 657–661.

Desikan RS, Ségonne F, Fischl B, Quinn BT, Dickerson BC, Blacker D, et al. An automated labeling system for subdividing the human cerebral cortex on MRI scans into gyral based regions of interest. Neuroimage 2006; 31: 968 980.

Fortea J, Sala-Llonch R, Bartrés-Faz D, Bosch B, Lladó A, Bargalló N, et al. Increased Cortical Thickness and Caudate Volume Precede Atrophy in PSEN1 Mutation Carriers. J Alzheimer's Dis 2010; 22: 909–922.

Fortea J, Vilaplana E, Alcolea D, Carmona-Iragui M, Sánchez-Saudinos M-B, Sala I, et al. Cerebrospinal fluid β-amyloid and phospho-tau biomarker interactions affecting brain structure in preclinical Alzheimer disease. Ann Neurol 2014; 76: 223–230.

Fukutomi H, Glasser MF, Zhang H, Autio JA, Coalson TS, Okada T, et al. Neurite imaging reveals microstructural variations in human cerebral cortical gray matter. Neuroimage 2018; 182: 488–499.

Garyfallidis E, Brett M, Amirbekian B, Rokem A, Walt S van der, Descoteaux M, et al. Dipy, a library for the analysis of diffusion MRI data. Front Neuroinform 2014; 8: 8.

Gauthier S, Albert M, Fox N, Goedert M, Kivipelto M, Mestre-Ferrandiz J, et al. Why has therapy development for dementia failed in the last two decades? Alzheimer's Dementia 2015; 12: 60–64.

Glasser MF, Sotiropoulos SN, Wilson JA, Coalson TS, Fischl B, Andersson JL, et al. The minimal preprocessing pipelines for the Human Connectome Project. Neuroimage 2013; 80: 105–124.

Grussu F, Schneider T, Tur C, Yates RL, Tachrount M, Ianuş A, et al. Neurite dispersion: a new marker of multiple sclerosis spinal cord pathology? Ann Clin Transl Neur 2017; 4: 663–679.

Guerrero JM, Adluru N, Bendlin BB, Goldsmith HH, Schaefer SM, Davidson RJ, et al. Optimizing the intrinsic parallel diffusivity in NODDI: An extensive empirical evaluation. Plos One 2019; 14: e0217118.

Henf J, Grothe MJ, Brueggen K, Teipel S, Dyrba M. Mean diffusivity in cortical gray matter in Alzheimer's disease: The importance of partial volume correction. Neuroimage Clin 2018; 17: 579–586.

Iacono D, Markesbery WR, Gross M, Pletnikova O, Rudow G, Zandi P, et al. The Nun Study: Clinically silent AD, neuronal hypertrophy, and linguistic skills in early life. Neurology 2009; 73: 665–673.

Iacono D, O'Brien R, Resnick SM, Zonderman AB, Pletnikova O, Rudow G, et al. Neuronal hypertrophy in asymptomatic Alzheimer disease. J Neuropath Exp Neur 2008; 67: 578–89.

Jack CR, Bennett DA, Blennow K, Carrillo MC, Dunn B, Haeberlein SB, et al. NIA-AA Research Framework: Toward a biological definition of Alzheimer's disease. Alzheimer's Dementia J Alzheimer's Assoc 2018; 14: 535–562.

Jack CR, Knopman DS, Jagust WJ, Petersen RC, Weiner MW, Aisen PS, et al. Tracking pathophysiological processes in Alzheimer's disease: an updated hypothetical model of dynamic biomarkers. Lancet Neurology 2013; 12: 207 216.

Jack CR, Vemuri P, Wiste HJ, Weigand SD, Aisen PS, Trojanowski JQ, et al. Evidence for ordering of Alzheimer disease biomarkers. Arch Neurol-chicago 2011; 68: 1526–35.

Jack CR, Wiste HJ, Therneau TM, Weigand SD, Knopman DS, Mielke MM, et al. Associations of Amyloid, Tau, and Neurodegeneration Biomarker Profiles With Rates of Memory Decline Among Individuals Without Dementia. Jama 2019; 321: 2316.

Jacobs HIL, Boxtel MPJ van, Gronenschild EHBM, Uylings HBM, Jolles J, Verhey FRJ. Decreased gray matter diffusivity: A potential early Alzheimer's disease biomarker? Alzheimer's Dementia 2013; 9: 93–97.

Jespersen SN, Bjarkam CR, Nyengaard JR, Chakravarty MM, Hansen B, Vosegaard T, et al. Neurite density from magnetic resonance diffusion measurements at ultrahigh field: Comparison with light microscopy and electron microscopy. Neuroimage 2010; 49: 205–216.

Johnson SC, Koscik RL, Jonaitis EM, Clark LR, Mueller KD, Berman SE, et al. The Wisconsin Registry for Alzheimer's Prevention: A review of findings and current directions. Alzheimer's Dementia Diagnosis Assess Dis Monit 2018; 10: 130 142.

Joie RL, Bejanin A, Fagan AM, Ayakta N, Baker SL, Bourakova V, et al. Associations between [18 F]AV1451 tau PET and CSF measures of tau pathology in a clinical sample. Neurology 2017; 90: e282–e290.

Kellner E, Dhital B, Kiselev VG, Reisert M. Gibbs-ringing artifact removal based on local subvoxel-shifts. Magnet Reson Med 2016; 76: 1574–1581.

Klein A, Tourville J. 101 Labeled Brain Images and a Consistent Human Cortical Labeling Protocol. Front Neurosci-switz 2012; 6: 171.

Lewczuk P, Lelental N, Spitzer P, Maler JM, Kornhuber J. Amyloid-β 42/40 cerebrospinal fluid concentration ratio in the diagnostics of Alzheimer's disease: validation of two novel assays. J Alzheimer's Dis 2015; 43: 183 191.

Lifke V, Kollmorgen G, Manuilova E, Oelschlaegel T, Hillringhaus L, Widmann M, et al. Elecsys® Total-Tau and Phospho-Tau (181P) CSF assays: Analytical performance of the novel, fully automated immunoassays for quantification of tau proteins in human cerebrospinal fluid. Clin Biochem 2019; 72: 30–38.

Mak E, Bethlehem RAI, Romero-Garcia R, Cervenka S, Rittman T, Gabel S, et al. In vivo coupling of tau pathology and cortical thinning in Alzheimer's disease. Alzheimer's Dementia Diagnosis Assess Dis Monit 2018; 10: 678–687.

Mangialasche F, Solomon A, Winblad B, Mecocci P, Kivipelto M. Alzheimer's disease: clinical trials and drug development. Lancet Neurology 2010; 9: 702–16.

Mattsson N, Schöll M, Strandberg O, Smith R, Palmqvist S, Insel PS, et al. (18)F-AV-1451 and CSF T-tau and P-tau as biomarkers in Alzheimer's disease. Embo Mol Med 2017; 9: 1212–1223.

Montal V, Vilaplana E, Alcolea D, Pegueroles J, Pasternak O, González-Ortiz S, et al. Cortical microstructural changes along the Alzheimer's disease continuum. Alzheimer's Dementia 2018; 14: 340 351.

Nazeri A, Chakravarty MM, Rotenberg DJ, Rajji TK, Rathi Y, Michailovich OV, et al. Functional Consequences of Neurite Orientation Dispersion and Density in Humans across the Adult Lifespan. J Neurosci 2015; 35: 1753–1762.

Nazeri A, Mulsant BH, Rajji TK, Levesque ML, Pipitone J, Stefanik L, et al. Gray Matter Neuritic Microstructure Deficits in Schizophrenia and Bipolar Disorder. Biol Psychiat 2017; 82: 726–736.

Parker TD, Slattery CF, Zhang J, Nicholas JM, Paterson RW, Foulkes AJM, et al. Cortical microstructure in young onset Alzheimer's disease using neurite orientation dispersion and density imaging. Hum Brain Mapp 2018; 39

Pegueroles J, Vilaplana E, Montal V, Sampedro F, Alcolea D, Carmona-Iragui M, et al. Longitudinal brain structural changes in preclinical Alzheimer's disease. Alzheimer's Dementia 2016; 13: 499–509.

Pierpaoli C, Jezzard P, Basser PJ, Barnett A, Chiro GD. Diffusion tensor MR imaging of the human brain. Radiology 1996; 201: 637–648.

Praet J, Manyakov NV, Muchene L, Mai Z, Terzopoulos V, Backer S de, et al. Diffusion kurtosis imaging allows the early detection and longitudinal follow-up of amyloid-β-induced pathology. Alzheimer's Res Ther 2018; 10: 1.

Riudavets MA, Iacono D, Resnick SM, O'Brien R, Zonderman AB, Martin LJ, et al. Resistance to Alzheimer's pathology is associated with nuclear hypertrophy in neurons. Neurobiol Aging 2007; 28: 1484–1492.

Scheff SW, Price DA, Schmitt FA, Scheff MA, Mufson EJ. Synaptic Loss in the Inferior Temporal Gyrus in Mild Cognitive Impairment and Alzheimer's Disease. J Alzheimer's Dis 2011; 24: 547–557.

Schwarz CG, Gunter JL, Wiste HJ, Przybelski SA, Weigand SD, Ward CP, et al. A large-scale comparison of cortical thickness and volume methods for measuring Alzheimer's disease severity. Neuroimage Clin 2016; 11: 802 812.

Smith SM, Jenkinson M, Johansen-Berg H, Rueckert D, Nichols TE, Mackay CE, et al. Tract-based spatial statistics: Voxelwise analysis of multi-subject diffusion data. Neuroimage 2006; 31: 1487–1505.

Smith SM, Nichols TE. Threshold-free cluster enhancement: Addressing problems of smoothing, threshold dependence and localisation in cluster inference. Neuroimage 2009; 44: 83–98.

Sperling RA, Aisen PS, Beckett LA, Bennett DA, Craft S, Fagan AM, et al. Toward defining the preclinical stages of Alzheimer's disease: Recommendations from the National Institute on Aging-Alzheimer's Association workgroups on diagnostic guidelines for Alzheimer's disease. Alzheimer's Dementia 2011; 7: 280–292.

Sperling RA, Mormino EC, Schultz AP, Betensky RA, Papp KV, Amariglio RE, et al. The impact of Aβ and tau on prospective cognitive decline in older individuals. Ann Neurol 2018; 85: 181–193.

Vanhoutte G, Pereson S, Palacios RD y, Guns P-J, Asselbergh B, Veraart J, et al. Diffusion kurtosis imaging to detect amyloidosis in an APP/PS1 mouse model for Alzheimer's disease. Magnet Reson Med 2013; 69: 1115–1121.

Veraart J, Novikov DS, Christiaens D, Ades-aron B, Sijbers J, Fieremans E. Denoising of diffusion MRI using random matrix theory. Neuroimage 2016; 142: 394–406.

Vogt NM, Hunt JF, Adluru N, Dean DC, Johnson SC, Asthana S, et al. Cortical Microstructural Alterations in Mild Cognitive Impairment and Alzheimer's Disease Dementia. Cereb Cortex 2020

Weston PSJ, Simpson IJA, Ryan NS, Ourselin S, Fox NC. Diffusion imaging changes in grey matter in Alzheimer's disease: a potential marker of early neurodegeneration. Alzheimer's Res Ther 2015; 7: 47.

Winkler AM, Ridgway GR, Webster MA, Smith SM, Nichols TE. Permutation inference for the general linear model. Neuroimage 2014; 92: 381–397.

Yotter RA, Dahnke R, Thompson PM, Gaser C. Topological correction of brain surface meshes using spherical harmonics. Hum Brain Mapp 2011a; 32: 1109–1124.

Yotter RA, Thompson PM, Gaser C. Algorithms to Improve the Reparameterization of Spherical Mappings of Brain Surface Meshes. J Neuroimaging 2011b; 21: e134–e147.

Zhang H, Schneider T, Wheeler-Kingshott CA, Alexander DC. NODDI: practical in vivo neurite orientation dispersion and density imaging of the human brain. Neuroimage 2012; 61: 1000 1016.

Figure Legends

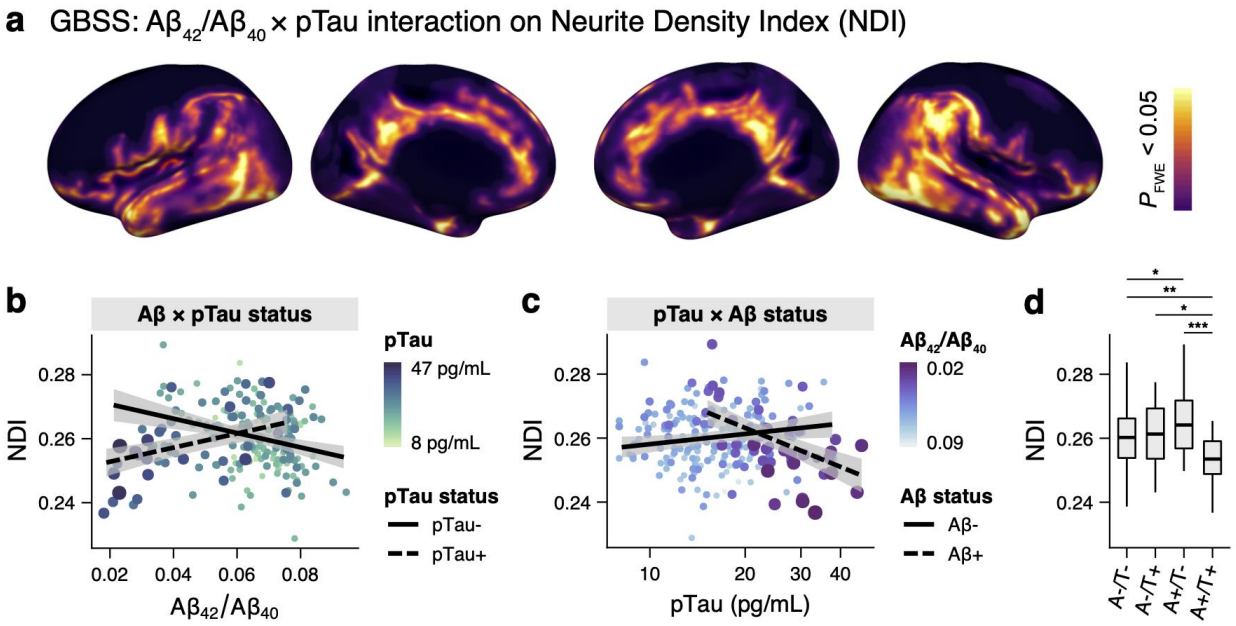

Figure 1. Gray matter-based spatial statistics (GBSS) results showing a significant Aβ$_{42}$/Aβ$_{40}$ × pTau interaction on cortical neurite density index (NDI). (a) Overlay of significant (FWE-corrected $P < 0.05$) GBSS results on inflated surface projection. **(b-c)** Mean NDI values from significant GBSS voxels were extracted in native diffusion space for each participant and plotted as scatter plots. Points are sized and colored by the moderator variable, and fit lines represent conditional slopes from simple slopes analyses. **(b)** For Aβ × pTau status, there was a significant negative conditional slope of Aβ$_{42}$/Aβ$_{40}$ on NDI at the pTau- group and a significant positive conditional slope at the pTau+ group mean. **(c)** For pTau × Aβ status, there was a significant positive conditional slope of pTau on NDI at the Aβ- group and a significant negative conditional slope at the Aβ+ group mean. **(d)** NDI values were collapsed across biomarker groups and ANCOVA models showed that the A+/T- group had higher NDI than the A-/T- group, and the A+/T+ group had lower NDI than all other groups. *$P < 0.05$, **$P < 0.01$, ***$P < 0.001$

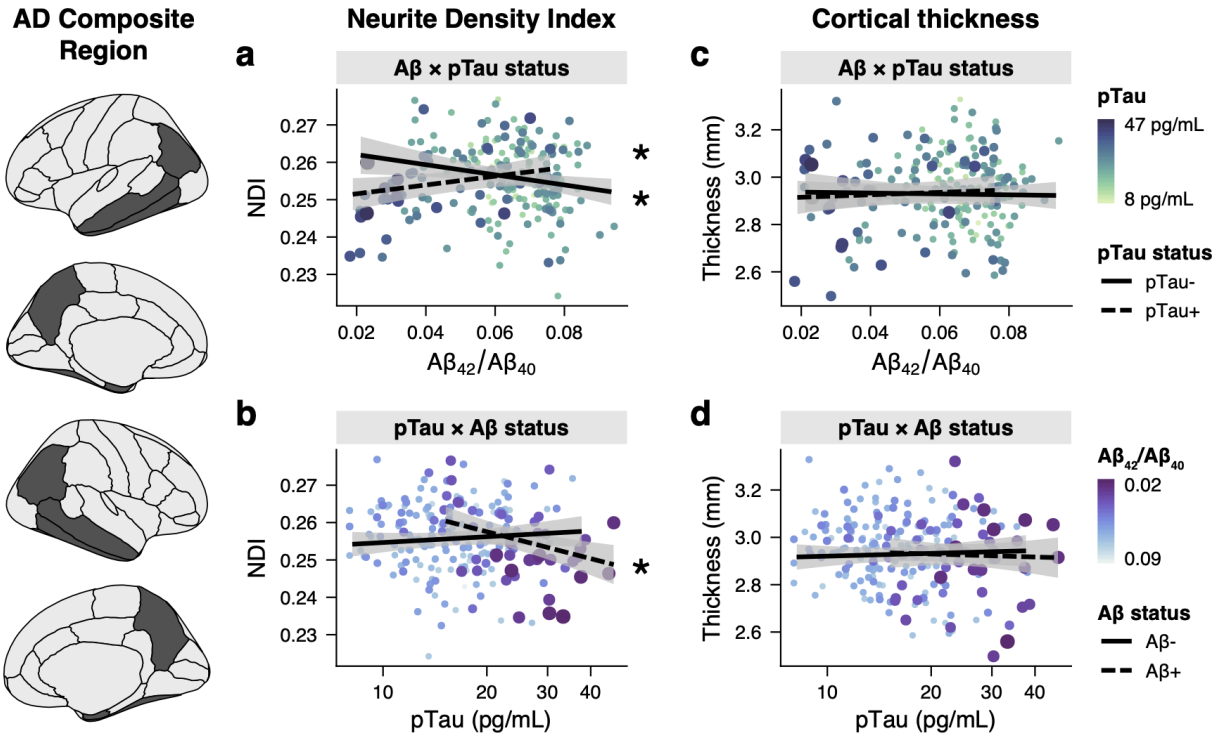

Figure 2. Interaction of $A\beta_{42}/A\beta_{40}$ × pTau for neurite density index (NDI) and cortical thickness values extracted from Alzheimer's disease (AD) composite region. Mean NDI or cortical thickness were extracted from a bilateral Alzheimer's disease composite region and plotted as scatter plots. Points are sized and colored by the moderator variable, and fit lines represent conditional slopes from simple slopes analyses. **(a)** For Aβ × pTau status, there was a significant negative conditional slope of $A\beta_{42}/A\beta_{40}$ on NDI at the pTau- group mean and a significant positive conditional slope at the pTau+ group mean. **(b)** For pTau × Aβ status, there was a significant negative conditional slope of pTau on NDI at the Aβ+ group mean, but no significant conditional slope at the Aβ- group mean. **(c-d)** There was no significant $A\beta_{42}/A\beta_{40}$ × pTau interaction on cortical thickness.

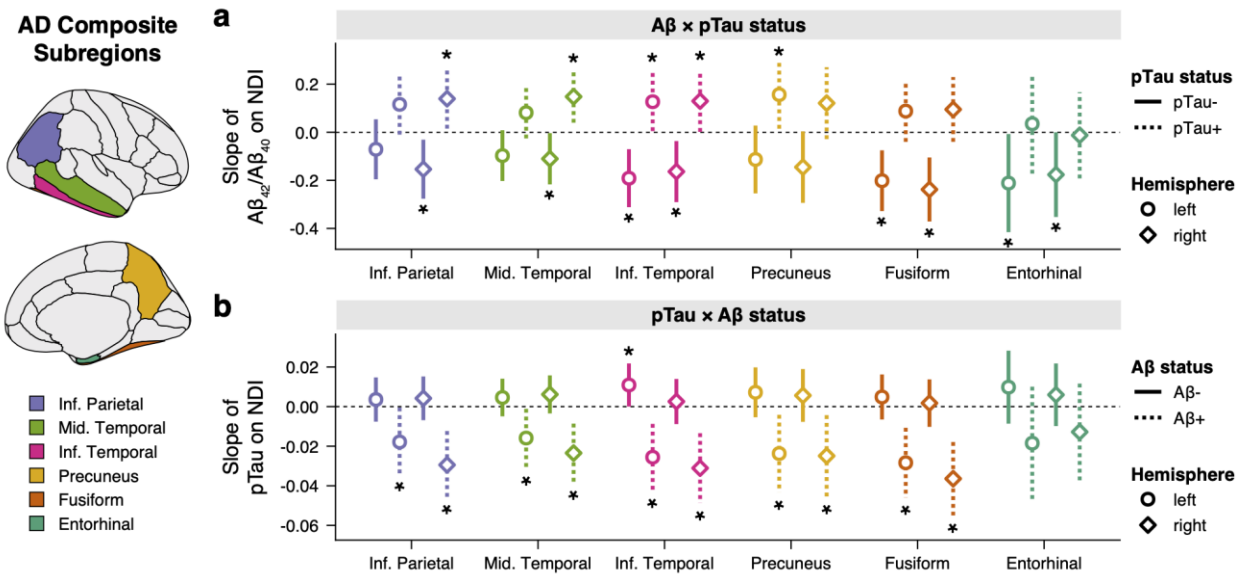

Figure 3. Regional patterns of $A\beta_{42}/A\beta_{40}$ × pTau interaction effects on NDI in the Alzheimer's composite subregions. Estimates of conditional slopes (with 95% confidence intervals) for each subregion and hemisphere. *$P < 0.05$ (uncorrected). **(a)** For Aβ × pTau status, subregions showed negative conditional slopes of $A\beta_{42}/A\beta_{40}$ on NDI at the pTau- group mean and positive conditional slopes of $A\beta_{42}/A\beta_{40}$ on NDI at the pTau+ group mean, indicating that greater amyloid burden was associated with higher NDI in pTau- individuals and lower NDI in pTau+ individuals. **(b)** For pTau × Aβ status, all subregions (except entorhinal) showed negative conditional slopes of pTau on NDI at the Aβ+ group mean, indicating that higher CSF pTau levels were associated with lower NDI in Aβ+ individuals.